On the Solved Turbulent Scales in Turbulent Plume Fires

On the Solved Turbulent Scales in Turbulent Plume Fires

F.S. Ciani[1], P. Bonfiglio[2] and S. Piva[1]

[1] Department of Engineering DE, Università di Ferrara, Via Saragat 1, 44122 Ferrara
[2] Materiacustica Srl, Via Saragat 1, 44122 Ferrara, Italy

pvs@unife.it

Abstract. Plume fires are characterized by a turbulent nature with a large number of different scales. LES is often used to solve the largest structures and to model the smallest ones. Grid size and time steps become decisive to place the limit between resolved and modelled turbulence. Significant information on this limit and its placement can be obtained with spectral analyses of the specific turbulent kinetic energy. While frequency analysis is relatively easy, an analysis in the wavenumber domain is more challenging. The IWC method, typically used in structures and acoustics, is used here for this purpose. IWC method allows to obtain wavenumber spectra with a better resolution than those obtained with a direct approach. Furthermore, in this paper the IWC method is also used in its reverse form to obtain frequency spectra. Although rather dense grids have been chosen, the number of nodes along the plume and their spacing is not such as to guarantee detailed wavenumber spectra with the direct approach and consequently with the reverse IWC. On the contrary, the IWC method provides wavenumber spectra in agreement with those obtained directly, but of much higher quality.

1. Introduction

The freeware CFD code “Fire Dynamics Simulator” (FDS) is an LES CFD code capable of capturing the time evolution of a fire and its turbulent nature. The LES approach allows to resolve the largest eddies and to model the smallest ones. The resolved scale is generally proportional to the size of the grid cells and of the time intervals: the smaller they are, the smaller the resolved scale. This means that a large number of cells and time steps are required to resolve highly turbulent flows and capture a significant number of turbulent structures. It is therefore important to understand where the bound between resolved and modelled turbulence is placed. Significant information on this limit and its location can be obtained with spectral analyses, in particular of the specific turbulent kinetic energy (*tke* in the following). These spectra can be studied both in time and in space. In the time domain a frequency analysis is required, while in the space domain a wavenumber analysis is required. If a frequency analysis simply involves the Fourier transform on time-varying data sets, usually largely available, in the wavenumber domain the methodology for obtaining the spectra is more challenging.

The main method for the computation of spectra in the wavenumber domain is the direct approach, which goes through “the spatial correlation function” between the fluctuations of velocity at a certain instant in a point and in the surroundings. However, in using the direct approach, a difficulty stems from the need of data in a large number of closely spaced points, usually not available. As an alternative to the direct approach, the spectra in the wavenumber domain were obtained using the Taylor’s Hypothesis (TH), relating spatial and temporal characteristics of turbulence [1]. Beside TH, in the literature several approaches were proposed to analyse the spectra in the wavenumber domain, such as different corrections to TH [2], and the models derived from the random sweeping hypothesis [3,4]

A new investigation approach for spectra in the wavenumber domain can be followed using the "Inhomogeneous wave correlation" (IWC) method [5]. The IWC method, starting from the frequency spectra calculated in a certain number of points of the domain, allows to obtain the so-called correlation-fit, i.e. a correlation between frequencies and wavenumbers valid along the path where the frequency spectra are made available. In [5], presumably the first application of the IWC method to turbulence, for a test case of turbulent reacting plumes, *tke* is analysed both in frequencies and wavenumbers and a correlation is found between these parameters.

In the present paper we continue the research started in [5]. A refined grid allows to broaden the range of frequencies and wavenumbers under examination. The intention is to highlight the correlations between grid spacing, time steps and resolved turbulence scales, by means of the *tke* spectra along the centreline of the fire plume. Particular attention is given to the grid spacing. As a starting point, the rule of thumb for the grid recommended by the FDS User Guide [6] is used, consisting in a suggested ratio between the characteristic diameter of the fire and the grid size. Furthermore, it is verified whether the above-mentioned energy spectra exhibit the scaling laws in the inertial subrange and follow the Kolmogorov theory. Furthermore, a study is performed to evaluate the effect of the grid spacing on the *tke* spectra. In addition, we reverse the procedure to examine the results obtained by starting from spectra in the wavenumber domain to obtain the corresponding in the frequency domain.

2. Case Study and Methodology

The plume of a turbulent fire in a cubic domain (10 m side) is considered as the case study (Fig. 1). Top and bottom surfaces are solid walls. The side faces are free to communicate with the external environment. A square burner (L = 1.5 m) is hosted in the centre of the lower plane on a 0.5 m high support. Propane, released at such a flow rate as to achieve an assigned heat release rate (*HRR*), is used as the fuel for the fire. The *HRR* curve reaches, with a linear growth, a maximum power of 5 MW after 10 s (Fig. 2).

The fire problem is addressed numerically using the CFD code FDS release 6.7.1. Compared to what presented in [5], the grid has been modified using the multi-block option with refinements in the areas of interest (plume, ceiling jet), to further halve the finest mesh size previously analysed. The case study is then studied for two different meshes (finer grid size: 0.0625 and 0.03125 m, respectively; larger grid size 0.25 m). Overall, grids of 912 10^3 and 6940 10^3 nodes are generated. The choice of the larger grid (0.25 m) is based on the rule of thumb proposed in the FDS User Guide [6]. For all the runs a constant time step of 10^{-3} s is chosen, having always checked that the stability constraints are satisfied. No slip conditions are assigned to the bottom and top walls. The remaining faces are modelled as openings where the fluid can enter or exit. On these open boundaries, conditions of constant total pressure are assumed. The wind velocity in the far field is zero. It is assumed that the bottom and top walls and the side surfaces of the burner are inert. The LES approach with the Deardorff sub-grid model is used to perform turbulence computations.

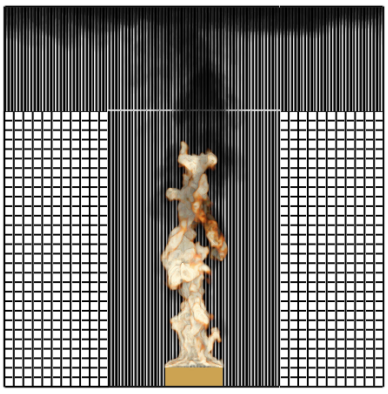

Figure 1: Computational grid.

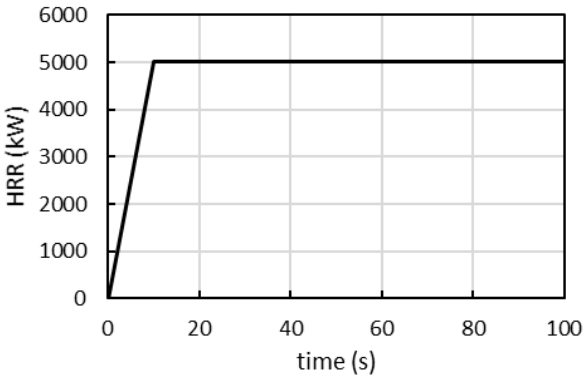

Figure 2: HRR imposed to the burner.

A detailed description of the IWC method is given in [5]. The IWC method is commonly applied to obtain *tke* spectra in the wavenumber domain. To do this, frequency spectra for the points along the centreline are produced as the first step. Next, the IWC method is applied to obtain a correlation between frequencies and wavenumbers. Finally, the wavenumber spectra are obtained by applying the correlation to the frequency spectra.

To deepen the knowledge about the IWC method here we use it in a reverse way, to obtain the *tke* spectra in the frequency domain. In more details, while in [5] the IWC method was used following the standard approach (it means from frequencies to wavenumbers), here we reverse the approach starting from wavenumber spectra calculated through FFTs of the spatial distribution of *tke* at different times. Afterwards, the correlation between frequencies and wavenumbers is obtained with the IWC method. Finally, the frequency spectra are obtained by applying the correlation to the wavenumber spectra.

3. Results and Discussion

The velocity components $\tilde{u}_i\,(\bar{x},t)$ are recorded at each node along the vertical centreline (x_3) of the plume, starting from 1 m up to 9 m (1 m from the ceiling). The Reynolds decomposition is applied to the velocity components $\tilde{u}_i\,(\bar{x},t)$. For example, in the time interval $20 \leq t \leq 100$ s, time-averaged velocities, $U_i\,(\bar{x})$, and velocity fluctuations, $u_i\,(\bar{x},t)$, are separated. In this interval the time average of the velocity fluctuations tends to 0. Next, from the velocity fluctuations, the history of $tke(\bar{x},t)$ along the centreline of the domain is calculated.

3.1. Spectra in the wavenumber domain

The data of *tke* at a point $\bar{x}_0$, $tke(\bar{x}_0,t)$, are the basic elements for the search of the frequency spectra, $TKE(\bar{x},f)$. These are computed with an FFT algorithm. Since the time step is 10^{-3} s, the corresponding Nyquist frequency is 500 Hz.

In Figure 3 the numerical results for the two grids are presented in terms of frequency spectra of *tke* at a point. These spectra refer to a centreline cell at a height of 5 m ($x_3/D = 3$, where for the square burner $D = L$). In these *tke* spectra, the -2/3 power law of the Kolmogorov decay (-5/3 is the exponent of the corresponding Kolmogorov power spectra), shown by a reference line in Fig. 3, is a dominant feature. The inertial sub-range is captured for both the grids.

In FDS an implicit grid filtering is used. The filter size is the mesh spacing, uniform in this case study. The cutoff frequency, *i.e.* the frequency threshold between resolved and modelled turbulence, is placed where the sharp decrease declines. Necessarily this cutoff moves forward as the grid spacing decreases. In particular, the cutoff frequency is identified at approximately 100 Hz for $\Delta x = 0.0625$ m, and at 220 Hz for $\Delta x = 0.03125$ m.

The correlation between frequencies and streamwise wavenumbers, k_{p3}, is then investigated using

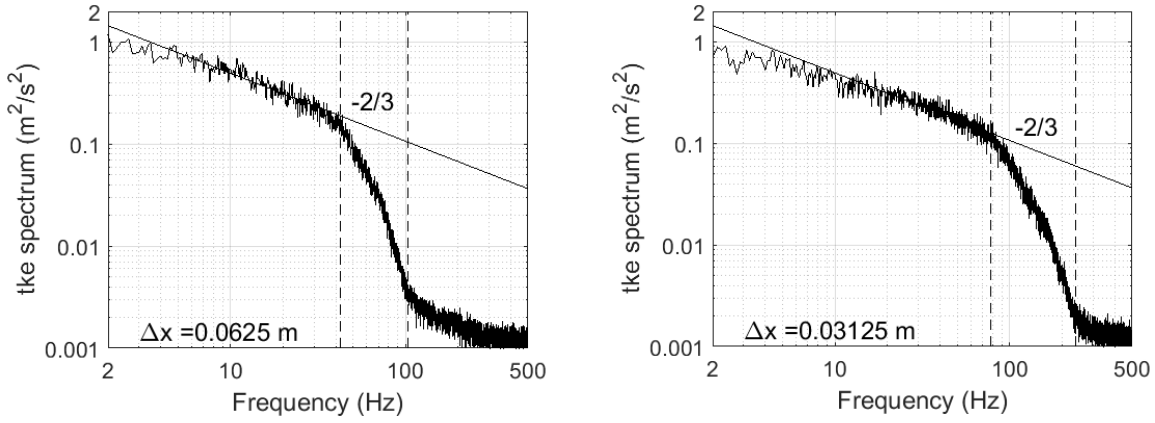

Figure 3: Frequency spectra of *tke* at 5 m of height.

the IWC method [1]. The frequency spectra are then reduced to obtain a correlation between f and k_{p3} (correlation-fit in the following). The results of this data reduction are presented in Fig. 4. The graph shows an area characterized by a high correlation, the "propagation area", and an area of low correlation, the "non-propagation area". In Figure 5, the data are presented for the two different grids with the fitting of the data set pertaining the finest grid. A linear fitting does not fit the two propagation areas. This means that in this case of reactive turbulent plume, Taylor's hypothesis cannot be applied. Conversely, a ratio of polynomials fits well the data in the propagation area. For frequencies tending to 0, the wavenumber values tend to 0. Finally, in Figure 5 the correlation-fit of the finer grid shows a good agreement also with the data set pertaining the coarser grid.

In Figure 6 the wavenumber spectra of *tke* produced by using the correlation-fit of Fig. 5 are presented. Qualitatively the spectra are very similar to those presented in Fig. 3. In both graphs a cutoff wavenumber is well evident, for increasing values when the grid reduces. These cutoff wavenumbers are in accordance with the Nyquist wavenumber, $k_C = \pi/\Delta x$, where Δx is the grid spacing. As for the frequency spectra of *tke* (Fig. 3), the $-2/3$ power law of the Kolmogorov decay, shown in Fig. 6 by a reference line, is a dominant feature and the inertial sub-range is captured for both grids.

3.2. Spectra in the frequency domain (reverse IWC method)

The IWC method can also be applied to obtain the *tke* spectra in the frequency domain from spectra in the wavenumber domain. This approach will be labelled "reverse IWC method".

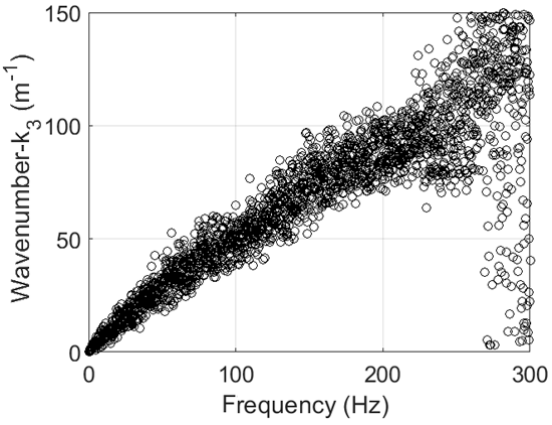

Figure 4: Data distribution (k_{p3}, f) for Δx = 0.03125 m.

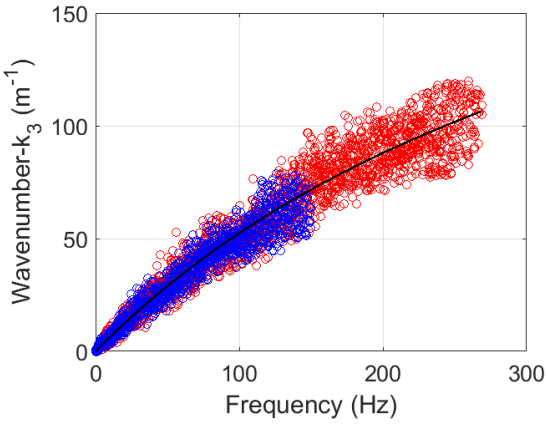

Figure 5: The correlation-fit on the two different grids.

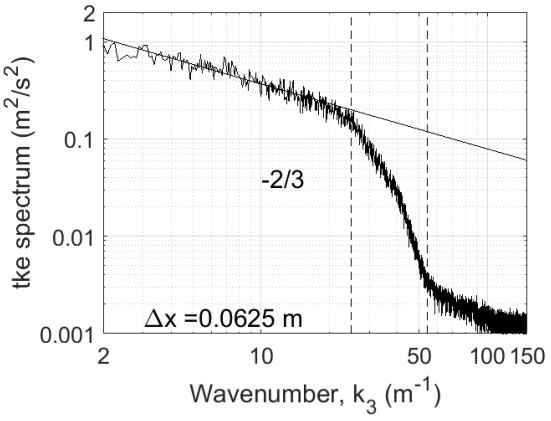

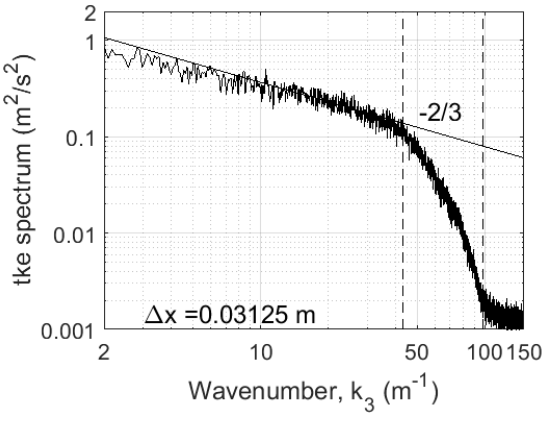

Figure 6: Wavenumber spectra of *tke* along the centreline.

The path for the application of the reverse IWC method is $20 \leq t \leq 100$ s. Since the grid steps are 0.0625 and 0.03125 m and the number of points along the path 128 and 256, respectively, the corresponding Nyquist wavenumbers are 50 and 100 m^{-1}.

The data of *tke* at an instant t_k, $tke(x_3,t_k)$, are the starting elements for the search for the wavenumber spectra, $TKE(k_{p3},t_k)$. To do it, an FFT in the space domain is performed:

$$TKE(k_{p3}, t_k) = \mathrm{FFT}(tke(x_3, t_k)) \tag{1}$$

The FFT is performed on the data available along the centre-line of the plume from 1 m up to 9 m (1 m from the ceiling).

The IWC method consists in evaluating the degree of consistency between the signal under examination, $TKE(k_{p3}, t_k)$, and an inhomogeneous wave (plane in this case):

$$\alpha(f_j, t_k) = \mathrm{A}\ \exp(-i\ 2\pi f_j\ t_k) \tag{2}$$

Dissipation is assumed to be negligible. The comparison is performed by calculating the indicator IWC for each element, $k_{p3,n}$, of the vector $TKE(k_{p3}, t_k)$:

$$IWC(f_j, k_{p3,n}) = \frac{\left| \sum_{k=1}^{K} \mathrm{A}\, e^{i\,(2\pi f_j t_k\ )} \cdot TKE(k_{p3,n}, t_k) \right|}{\sqrt{\sum_{k=1}^{K} \left| \mathrm{A}\, e^{i\,(-2\pi f_j t_k\ )} \right|^2 \sum_{k=1}^{K} \left| TKE(k_{p3,n}, t_k) \right|^2}} \tag{3}$$

Now, we can identify the stream-wise propagative wavenumbers by looking for the maximum of the IWC parameter among those calculated with Eq. (3) for each $k_{p3,n}$ as f_j varies. A dataset that relates k_{p3} with f allows us to obtain a correlation between these parameters.

In Figure 7 the results for the two grids are presented in terms of wavenumber spectra of *tke* at an instant (60 s). In these *tke* spectra, the inertial sub-range is captured and the -2/3 power law of the Kolmogorov decay (-5/3 is the exponent of the Kolmogorov power spectra), shown by a reference line in Fig. 7, is a dominant feature. The quality of the spectra is very low due to the limited number of grid points (128 and 256) available for the computations. The implicit grid filtering used by FDS in its LES implementation is barely visible. On the contrary, in both graphs the cutoff wavenumber, *i.e.* the threshold between resolved and modelled turbulence, is clearly visible. The spectra stop at the Nyquist wavenumbers (50 and 100 m^{-1}) given by $k_C = \pi/\Delta x$, where Δx is the grid spacing. Necessarily, these cutoff wavenumbers advance when the grid becomes finer.

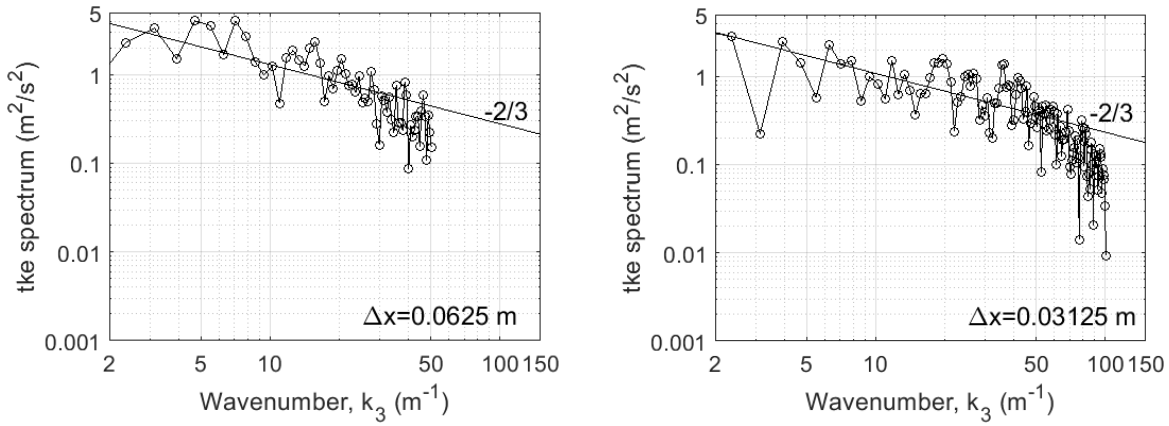

Figure 7: Wavenumber spectra of *tke* at 60 s.

The wavenumber spectra are reduced with the procedure given be Eqs. (1-3) to obtain the correlation-fit. The results of this data reduction are presented in Fig. 8. As expected, the data distribution becomes wider as the resolution of the grid increases. The data of both the distributions show a sharp discontinuity near half of the Nyquist wavenumber (25 and 50 m^{-1}). Both the distributions of data are overlapping up to half of the Nyquist wavenumber of the coarser grid.

In Figure 9 the correlation-fit pertinent to the finest grid is presented. Since the data show a sharp discontinuity near half of the Nyquist wavenumber, we interpolated up to this limit with a function consisting in a ratio of polynomials, as already done in [5]. Justifications for the extrapolation after this limit (dashed line) are addressed in Par. 3.3.

Finally, the correlation-fit is used to produce the frequency spectra of *tke*. In Figure 10 these spectra are presented for the two grids. Qualitatively the spectra are similar to those presented in Fig. 7. In both graphs a cutoff frequency is evident, for increasing values when the grid reduces. As for the wavenumber spectra of *tke* (Fig. 7), the −2/3 power law of the Kolmogorov decay, shown in Fig. 10 by a reference line, is a dominant feature and the inertial sub-range is captured for both grids. The attenuated region is barely visible.

Since the *tke* spectra (Figs. 7 and 10) are characterized by annoying fluctuations, which make the *tke* spectra difficult to read, an ensemble average of the wavenumber spectra at 50, 60, 70, 80 and 90 s is done. In Figure 11 these averaged spectra both in the wavenumber and in frequency domain are shown. Now the attenuated region becomes clearly visible. The lower bound of the attenuated region seems to

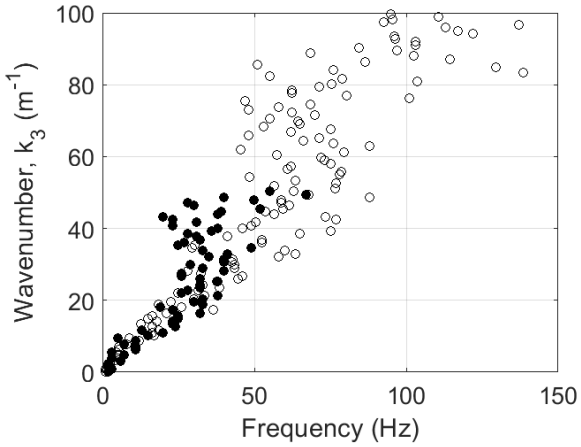

Figure 8: (k_{p3},f) data distributions for the grids.

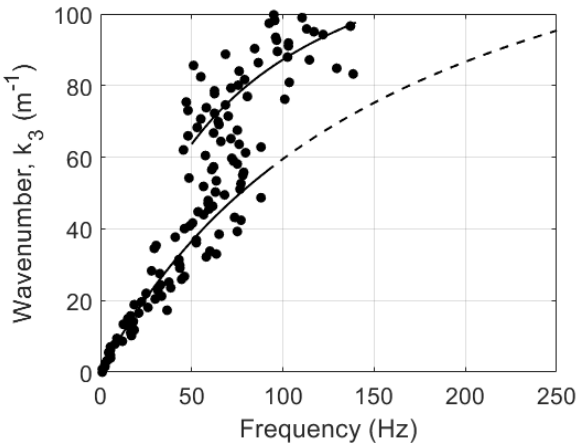

Figure 9: Correlation-fit for the finest grid.

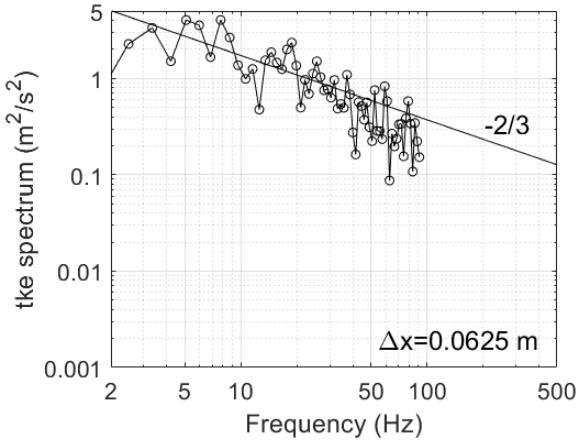

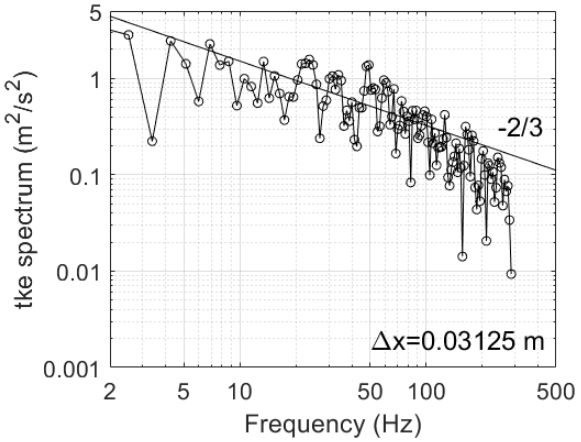

Figure 10: Frequency spectra of *tke* at 60 s.

coincide with half of the Nyquist wavenumber (25 and 50 m^{-1}). The upper bound of the attenuated region here coincides with Nyquist limits (50 and 100 m^{-1}) where the spectra stop. These cut-offs move forward when the grid becomes finer.

3.3. Procedures comparison

Here for the finest grid the results of the two procedures are compared and discussed. In Figure 12 the IWC parameter as a function of the frequency, for k_{p3} = 70 m^{-1}, is shown. These data are interpolated with a summation of Gaussian functions. This fitting allows to detect a second peak with a doubled mean, but with a lower scaling factor. The second Gaussian curve seems to detect the second harmonic of the inhomogeneous wave. In Figure 13, after the sharp discontinuity in frequency clearly visible in Fig. 9, the second harmonic of the IWC function is shown. In the same Figure, the correlation-fit obtained for the data of Fig. 9 is shown. This correlation fits well also the data after the half of the Nyquist number. This justifies our assumption of extrapolating the correlation-fit for the whole range of data of Fig. 13.

For these grids, when starting the procedure with the frequency spectra, the domain of validity of the correlation-fit is significantly larger. This is due to the limited number of points useful for computing the wavenumber spectra which limits the domain of validity of these spectra.

In Figure 14 the data obtained with the IWC method (Fig. 4) and with its reverse (Fig. 13) are compared. The number of data obtained by using the IWC method starting from the frequency spectra

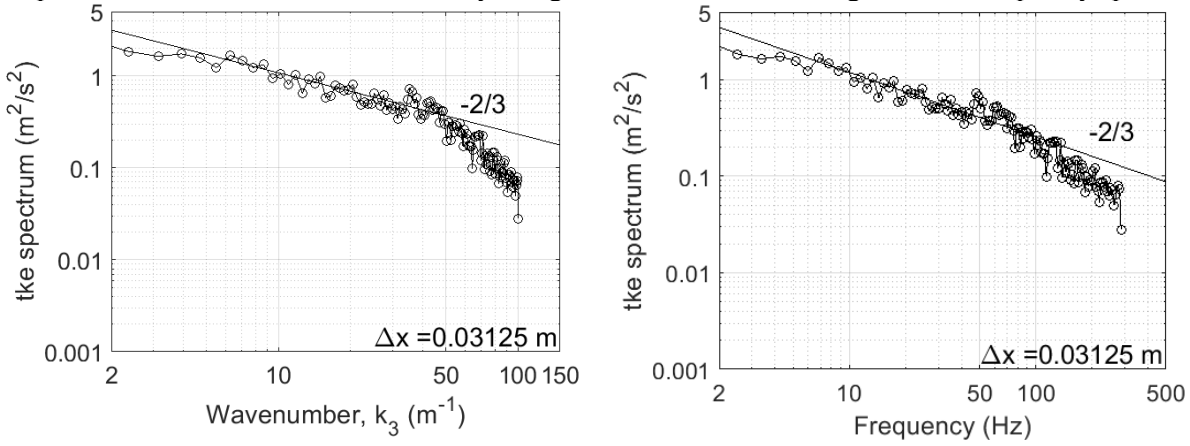

Figure 11 – Ensemble average of frequency and wavenumber spectra.

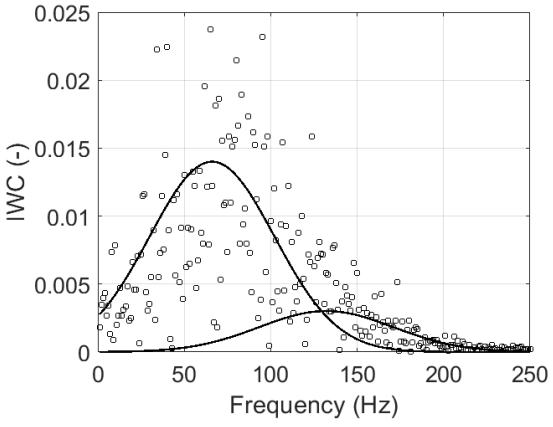

Figure 12 - IWC parameter at k_{p3} = 70 m^{-1}.

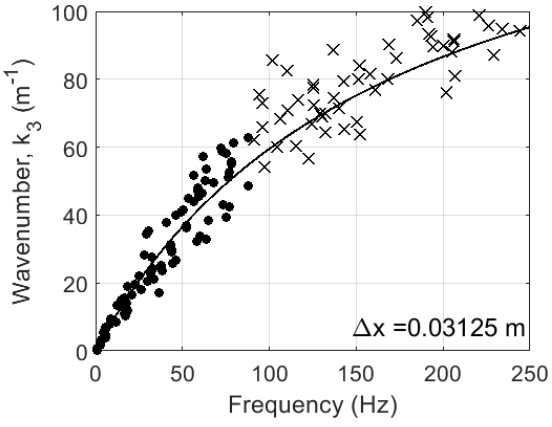

Figure 13 - Reverse IWC data: original (●) and shifted values (x)

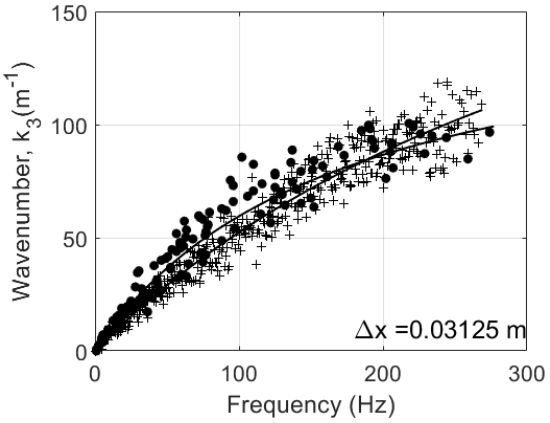

Figure 14 - Propagative dispersion graphs (wavenumber- (●) and frequency-spectra (+)).

is significantly larger than that obtained with the reverse IWC method. This is due to the limited number of points useful for computing the wavenumber spectra. Both the data sets are interpolated with the function $k = af / (f + b)$. The interpolation curves are quite similar. The one computed from the wavenumber spectra bends more sharply. Since the two data distributions of Fig. 14 shows an agreement, this can be a further justification for the data shift after the discontinuity shown in Fig. 8 and finally for the extrapolation.

Despite the large number of grid points (6940 10^3) the quality of the wavenumber spectra obtained with the direct approach (Fig. 7) or after an ensemble average (Fig. 11) is evidently lower than that given by the IWC method (Fig. 6).

4. Concluding Remarks

For a reacting turbulent flow, the IWC method is used to correlate the *tke* spectra in frequency and wavenumber domains. The analysis is carried out for two different grids. The Kolmogorov inertial subrange is always reached. The spectra drop sharply up to the frequency/wavenumber cutoff through an attenuated region, the latter due to the implicit filtering of the LES code.

With the IWC method, spectral analyses in the wavenumber domain become easy. Furthermore, the IWC method shows the interesting advantage of avoiding any physical model.

Even for a very fine grid like that used in this paper (6940 10^3), the number of nodes along the plume and their spacing are not enough to allow the reverse of the IWC method to produce information comparable to those produced with the standard IWC method.

References

[1] Taylor G I 1938 The spectrum of turbulence *Proc. R. Soc.* A **164** 476–490 doi: 10.1098/rspa.1938.0032

[2] Geng C, He G, Wang Y, Xu C, Lozano-Durán A and Wallace J M. 2015 Taylor's hypothesis in turbulent channel flow considered using a transport equation analysis. *Phys. Fluids* **27** 025111 doi: 10.1063/1.4908070

[3] Wilczek M and Narita Y 2012 Wave-number–frequency spectrum for turbulence from a random sweeping hypothesis with mean flow *Phys. Rev.* E, **86** 066308 doi: 10.1103/physreve.86.066308

[4] He G W and Zhang J B 2006 Elliptic model for space-time correlations in turbulent shear flows *Phys. Rev.* E **73** 055303(R) doi: 10.1103/physreve.73.055303

[5] Ciani F S, Bonfiglio P and Piva S 2021 IWC analysis of turbulent plume fires *TECNICA ITALIANA-Italian Journal of Engineering Science* **65** 196-200. doi: 10.18280/ti-ijes.652-408

NIST 2018 *Fire Dynamics Simulator User's Guide* Special Publication 1019 (Gaithersburg, MD, NIST)